

CFARnet: deep learning for target detection with constant false alarm rate

Tzvi Diskin, Yiftach Beer, Uri Okun and Ami Wiesel

Abstract—We consider the problem of target detection with a constant false alarm rate (CFAR). This constraint is crucial in many practical applications and is a standard requirement in classical composite hypothesis testing. In settings where classical approaches are computationally expensive or where only data samples are given, Bayesian and machine learning methodologies are advantageous. CFAR is less understood in these settings. To close this gap, we introduce a framework of CFAR constrained detectors. Theoretically, we prove that a CFAR constrained Bayes optimal detector is asymptotically equivalent to the classical generalized likelihood ratio test (GLRT). Practically, we develop a deep learning framework for fitting neural networks that approximate it. Experiments in both model based target detection and data-driven hyperspectral images demonstrates that the proposed CFARnet allows a flexible tradeoff between CFAR and accuracy. In many problems near CFAR detectors can be developed with a small loss in accuracy.

Index Terms—hypothesis testing, deep learning, target detection.

I. INTRODUCTION

The deep learning revolution has led many to apply machine learning methods to classical problems in all fields including statistics. Examples range from estimation [1–6] to detection [7–12]. Deep learning is a promising approach for developing high accuracy and low complexity alternatives when classical solutions are intractable. However, deep learning based methods lack some of the crucial guarantees that classical methods provide. In this paper, we focus on learning detectors for composite hypothesis testing. We show that current solutions lack the Constant False Alarm Rate (CFAR) requirement which enables users to tune the sensitivity of the detectors to different conditions and is critical in many applications. To close this gap, we provide a framework for learning accurate CFAR detectors.

Model-based detection theory begins with the simple hypothesis testing problem where a detector must decide between two fully specified distributions. The classical solution is the Likelihood Ratio Test (LRT) which is optimal in terms of maximizing the detection probability subject to a false alarm constraint. Composite hypothesis testing is a more challenging setting where the hypotheses involve unknown deterministic parameters. A CFAR detector is invariant to these parameters and has constant false alarm probabilities. This allows the user to set the thresholds *a priori*. A popular approach is the Generalized Likelihood Ratio Test (GLRT) which is defined by first estimating the unknown parameters and then plugging them into a standard LRT. GLRT performs well and is asymptotically CFAR when the model is exact and the number of unknowns is relatively small. Otherwise, it is generally

sub-optimal and may be computationally expensive. Some techniques were developed for designing CFAR detectors for specific families of distributions [13–15].

Data-driven classifiers are the machine learning counterpart to model-based detectors. Instead of using the statistical model directly, the goal is minimize the average error on a training dataset among a restricted class of classifiers. In simple settings with no unknown deterministic parameters, it is well known that the optimal Bayes classifier converges to the LRT with a specific false alarm rate [16, p. 78]. Learned classifiers can be interpreted as approximations to these optimal Bayes solutions. More advanced classifiers can also maximize the cumulative detection rate over a wide range of false alarms, also known as the (partial) area under the curve (AUC) [17–19]. Large deviation analysis is available in [20]. Consequently, there is a growing body of works on using machine learning for target detection. In the context of hyperspectral imagery, [11] introduced the use of support vector machines (SVM) and deep neural networks were proposed in [8]. In the context of radar detection, SVMs were considered in [10]. Specific CFAR radar detectors were developed by relying on CFAR features [21–23].

The main contributions of the paper are:

- We define a general framework for Bayesian and learning-based CFAR detectors that can be applied to arbitrary composite hypothesis testing.
- We analyze the asymptotic performance of the proposed detectors. We prove that the CFAR constrained Bayes detector is asymptotically equivalent to the popular GLRT.
- We develop CFARnet - a practical deep learning approach to fitting neural networks with CFAR constraints. To optimize CFARnet, we rely on empirical and differentiable distances that have recently become popular in unsupervised deep learning [24–26].

Our experiments show that CFARnet is approximately CFAR while paying a small price in terms of accuracy. First, we show this in the context of detecting a signal with unknown amplitude in non-Gaussian noise. Second, we turn to a more challenging adaptive detection problem with unknown Gaussian noise covariance but access to secondary data of noise-only samples, which can be used for estimation of the covariance of the noise [27–30]. The popular regularizing trick, also known as shrinkage or diagonal loading, improves detection accuracy but is non-CFAR [31, 32]. On the other hand, experiments show that CFARnet is both accurate and CFAR. Finally, we demonstrate the advantages of CFARnet in

target detection of a plastic material in hyperspectral imagery. Here too, CFARnet finds a tradeoff between accuracy and CFAR. Its advantages are evident when we examine the detection rates under a strict worst-case false alarm across the full image.

For completeness, we note that the CFAR notion is closely related to the topics of “fairness” and “out of distribution (OOD)” generalization which have recently attracted considerable attention in the machine learning literature, e.g., [33, 34]. CFAR can be interpreted as a fairness property with respect to the unknown deterministic parameters. The closest work is [35] which also enforces “equalized odds” using a distance between distributions. A main difference is that CFAR is a one-sided fairness property and requires equal rates only in the null hypothesis. Algorithmically, [35] compares the high dimensional joint distribution of the predictions and the unknown parameters, whereas we only consider the scalar distribution of the predictions. This makes our method significantly cheaper in terms of computational complexity. Indeed, we rely on a simple kernel based distance and do not require sophisticated adversarial networks.

II. PROBLEM FORMULATION

We consider a binary hypothesis test. Let \mathbf{x} be an observed random vector whose distribution $p(\mathbf{x}; \mathbf{z})$ depends on an unknown deterministic parameter \mathbf{z} . The value of \mathbf{z} defines two possible hypotheses

$$\begin{aligned} y = 0 : \quad \mathbf{z} \in \mathcal{Z}_0 \\ y = 1 : \quad \mathbf{z} \in \mathcal{Z}_1. \end{aligned} \quad (1)$$

It is customary to divide $\mathbf{z} = \{\mathbf{z}_r, \mathbf{z}_n\}$ into two components. The parameter \mathbf{z}_r is discriminative whereas \mathbf{z}_n is a nuisance parameter which is the same under either hypothesis.

Throughout the paper, we will illustrate the ideas using a simple and classical running example:

Example 1: Target detection when both the target amplitude and the noise scaling are unknown:

$$\mathbf{x} = A\mathbf{1} + \sigma\mathbf{n} \quad (2)$$

where $\mathbf{1}$ is a target vector of ones, \mathbf{n} is a random vector with independent and identically distributed (i.i.d.) $\mathcal{N}(0, 1)$ noise variables, $\mathbf{z} = [A, \sigma]$ are deterministic unknown parameters, and

$$\begin{aligned} \mathcal{Z}_0 &= \{\mathbf{z} : A = 0, \sigma \neq 0\} \\ \mathcal{Z}_1 &= \{\mathbf{z} : A \neq 0, \sigma \neq 0\} \end{aligned} \quad (3)$$

Here, A acts as a discriminative parameter that varies between the two hypotheses, whereas the noise variance σ^2 is a nuisance parameter which is identical in both. Throughout the paper, we will consider both cases when σ^2 is known and unknown.

The goal is to design a detector $\hat{y}(\mathbf{x}) \in \{0, 1\}$ as a function of \mathbf{x} that will identify the true hypothesis $y \in \{0, 1\}$.

Performance is measured in terms of probability of correct detection, also known as True Positive Rate (TPR):

$$\text{Pr}_{\text{TPR}}(\mathbf{z}) = \Pr(\hat{y}(\mathbf{x}) = 1; y = 1) \quad (4)$$

and probability of false alarm, also known as False Positive Rate (FPR):

$$\text{Pr}_{\text{FPR}}(\mathbf{z}) = \Pr(\hat{y}(\mathbf{x}) = 1; y = 0). \quad (5)$$

In practice, the user typically provides a false alarm constraint $\text{Pr}_{\text{FPR}} \leq \alpha$ that must be satisfied and the goal is to maximize Pr_{TPR} .

It is standard to consider decision functions of the form

$$\hat{y}(\mathbf{x}) = \mathbf{1}_{T(\mathbf{x}) \geq \gamma} = \begin{cases} 0 & T(\mathbf{x}) < \gamma \\ 1 & T(\mathbf{x}) \geq \gamma \end{cases} \quad (6)$$

where $T(\mathbf{x})$ is denoted as the **detector** function and γ is a **threshold** value. This structure allows users to tune the FPR by adjusting the threshold. Performance is usually visualized using the Receiver Operating Characteristic (ROC) which plots the TPR as a function of the FPR. In signal processing applications, users are often interested in a region of very low FPRs, e.g., $10^{-1} - 10^{-3}$ and the goal is to maximize the TPR probabilities in this area. Note that the ROC does not give a full specification of the detector as it assumes that the threshold is tuned to fit the level of the FPR in each point of the curve. This leads us to the a main challenge in detection theory, which is the unknown nuisance parameters under the null hypothesis $y = 0$, e.g., the unknown noise variance σ^2 in Example 1. The FPR is generally a function of these parameters and cannot be controlled without their knowledge. As a remedy it is often preferable to restrict the attention to CFAR detectors.

Definition 1. A detector $T(\mathbf{x})$ is CFAR if its FPR $\Pr(T(\mathbf{x}) > \gamma | \mathbf{z} \in \mathcal{Z}_0)$ is invariant to the value of $\mathbf{z} \in \mathcal{Z}_0$, for any threshold γ .

It is straightforward to see that the above definition is equivalent to invariance of the distribution of $T(\mathbf{x})$ to all $\mathbf{z} \in \mathcal{Z}_0$.

As we will review below, many classical detectors are CFAR or asymptotically CFAR. With the growing trend of switching to machine learning, the goal of this paper is to introduce a competing framework for learning CFAR detectors.

III. CLASSICAL DETECTORS

Traditionally, detectors were developed based on statistical models using likelihood ratios. In the simple case, all the parameters of the hypotheses are known (e.g., Example 1 if σ was known and A and had a single possible value under $y = 1$). In this case, hypothesis testing has an optimal solution known as the Likelihood Ratio Test (LRT) due to Neyman-Pearson lemma [16, p. 65]:

$$T_{\text{LRT}}(\mathbf{x}) = 2\log \frac{p(\mathbf{x}; \mathbf{z} = \mathbf{z}_1)}{p(\mathbf{x}; \mathbf{z} = \mathbf{z}_0)} \quad (7)$$

where the threshold γ is chosen to satisfy the false alarm (FPR) constraint.

The more realistic scenario is composite hypotheses testing where one or both of the hypotheses allow multiple possible values and there is no solution that is optimal for all of them simultaneously. A popular heuristic is the Generalized Likelihood Ratio Test (GLRT) that estimates the unknowns using the Maximum Likelihood (ML) technique and plugs them into the LRT detector [16, p. 200]:

$$T_{\text{GLRT}}(\mathbf{x}) = 2\log \frac{\max_{\mathbf{z} \in \mathcal{Z}_1} p(\mathbf{x}; \mathbf{z})}{\max_{\mathbf{z} \in \mathcal{Z}_0} p(\mathbf{x}; \mathbf{z})} \quad (8)$$

Setting the threshold to ensure a fixed Pr_{FPR} is not trivial. Fortunately, under regularity conditions, GLRT is asymptotically CFAR and its threshold can be set for all values of the unknown parameters simultaneously.

Returning to Example 1: If the level of the noise σ^2 is known (no nuisance parameters), then GLRT is simply

$$T_{\text{GLRT}}(\mathbf{x}) = \frac{(\mathbf{x}^T \mathbf{1})^2}{N\sigma^2}. \quad (9)$$

When σ^2 is unknown, (9) can still be used without the constant denominator. This will result in the same ROC performance but no CFAR. A better approach is the GLRT associated with an unknown σ^2 which can be derived as

$$T_{\text{GLRT}}(\mathbf{x}) = \frac{(\mathbf{x}^T \mathbf{1})^2}{\mathbf{x}^T \mathbf{x}}. \quad (10)$$

This GLRT guarantees both a similar ROC performance and a CFAR for any value of σ^2 . Indeed, the denominator of (10) can be interpreted as an estimator of the unknown variance, i.e., $\mathbf{x}^T \mathbf{x} \approx N\sigma^2$.

GLRT is probably the most popular solution to composite hypothesis testing. It gives a simple recipe that performs well under asymptotic conditions. Its main downsides are that it is sensitive to deviations from its theoretical model, it is generally sub-optimal under finite sample settings and that it may be computationally expensive. Both the numerator and denominator of the GLRT involve optimization problems that may be large scale, non-linear and non-convex. Therefore, there is an ongoing search for robust and low cost alternatives.

IV. BAYESIAN DETECTORS

In this section, we review the Bayesian approach to hypothesis testing [16, Sec. 6.4.1]. As expected, this approach does not lead to CFAR detectors. To close this gap, we introduce a CFAR constrained Bayesian detector. We then analyze the detectors under the classical large data record setting.

A competing approach to hypothesis testing is based on the Bayesian methodology. The latter differs in two aspects from the classical approach. First, the unknown parameters (y and \mathbf{z}) are random with known priors. As detailed in [16, Sec. 6.4.1] the choice of these priors is often difficult and practitioners resort to fictitious “flat” distributions which are

non informative. Second, performance is measured in terms of probability of error with respect to these priors:

$$\begin{aligned} \text{Pr}_{\text{ERR}}(T, \gamma) &= \text{Pr}(\mathbf{1}_{T \geq \gamma} \neq y) \\ &= \text{Pr}(y = 0) \int_{\mathbf{z} \in \mathcal{Z}_1} \text{Pr}_{\text{FPR}}(\mathbf{z}) d\mathbf{z} \\ &\quad + \text{Pr}(y = 1) \int_{\mathbf{z} \in \mathcal{Z}_0} (1 - \text{Pr}_{\text{TPR}}(\mathbf{z})) d\mathbf{z} \end{aligned} \quad (11)$$

Together, these lead to a well defined Bayes optimal detector which is also known as Bayesian LRT (BLRT):

$$\text{BLRT} : \min_{T, \gamma} \text{Pr}_{\text{ERR}}(T, \gamma) \quad (12)$$

Its solution is

$$\begin{aligned} T_{\text{BLRT}}(\mathbf{x}) &= 2\log \frac{p_1(\mathbf{x})}{p_0(\mathbf{x})} = 2\log \frac{\int_{\mathbf{z} \in \mathcal{Z}_1} p(\mathbf{x}; \mathbf{z}) p(\mathbf{z}) d\mathbf{z}}{\int_{\mathbf{z} \in \mathcal{Z}_0} p(\mathbf{x}; \mathbf{z}) p(\mathbf{z}) d\mathbf{z}} \\ \gamma_{\text{BLRT}} &= 2\log \frac{\text{Pr}(y = 0)}{\text{Pr}(y = 1)}. \end{aligned} \quad (13)$$

Originally, BLRT was designed to minimize the probability of error. However, practitioners often use it even when the underlying formulation is classical, by assigning fictitious priors to the unknown parameters. In simple hypotheses, BLRT is identical to LRT and the only difference is the thresholds. For any required FPR, BLRT with an appropriate threshold maximizes the TPR (independently of the chosen prior).

In the composite case, BLRT is less understood. Due to the integrals, it typically does not have an easy solution. Even in the simple Example 1, depending on the chosen priors, BLRT may have a complicated form. Moreover, it is not clear how it performs in terms of FPR and TPR, nor how it compares to GLRT. Experiments in different settings reveal that BLRT does not generally guarantee a CFAR. To close this gap, we introduce a new detector, called CLRT, which is Bayes optimal subject to a CFAR constraint:

$$\text{CLRT} : \begin{cases} \min_{T, \gamma} \text{Pr}_{\text{ERR}}(T, \gamma) \\ \text{s.t.} \quad T \text{ is CFAR} \end{cases} \quad (14)$$

In what follows, we claim that CLRT is the natural Bayesian version of GLRT. When there are no complicating nuisance parameters, BLRT and GLRT are asymptotically equivalent. Otherwise, the CFAR constraint in (14) is necessary and leads to equivalence between CLRT and GLRT. To formally state this result, we begin by recalling the classical large data records setup due to [16, p. 205]. We consider $\mathbf{x} \sim p(\mathbf{x}; \mathbf{z}_r, \mathbf{z}_n)$ and test

$$\begin{aligned} y = 0 : \quad &\mathbf{z}_r = \mathbf{z}_{r_0}, \mathbf{z}_n \\ y = 1 : \quad &\mathbf{z}_r \neq \mathbf{z}_{r_0}, \mathbf{z}_n, \end{aligned} \quad (15)$$

where $\mathbf{z}_r \in \mathbb{R}^{d_r}$ is a discriminative parameter and $\mathbf{z}_n \in \mathbb{R}^{d_n}$ is a nuisance parameter. We let \mathbf{z}_{r_0} and \mathbf{z}_{r_1} be the true values of \mathbf{z}_r at $y = 0$ and $y = 1$, respectively. We further assume that:

- The data consist of many i.i.d samples from the true statistical model:

$$p(\mathbf{x}; \mathbf{z}_r, \mathbf{z}_n) = \prod_{i=1}^N p(x_i; \mathbf{z}_r, \mathbf{z}_n). \quad (16)$$

- The signal is weak:

$$\|\mathbf{z}_{r_1} - \mathbf{z}_{r_0}\| = \frac{s}{\sqrt{N}}, \quad (17)$$

where s is some finite constant.

- The ML estimators of the unknown parameters are statistically efficient and attain their asymptotic performance.

Under these conditions, when $N \rightarrow \infty$, it is well known that GLRT attains its asymptotic performance. The next two theorems analyze BLRT and CLRT in the same setting. We first state the results and their consequences, and then provide the proofs.

Theorem 1. *Consider the classical asymptotic setting and assume the technical conditions as detailed in appendix A. Then, independently of the choice of $p(\mathbf{z})$ prior, we have*

$$T_{\text{BLRT}}(\mathbf{x}) \rightarrow T_{\text{GLRT}}(\mathbf{x}) + \text{func}(\mathbf{z}_{r_0}, \mathbf{z}_n). \quad (18)$$

The decomposition in (18) means that, if there are no nuisance parameters (no \mathbf{z}_n), then BLRT and GLRT are equivalent (since \mathbf{z}_{r_0} is known). Otherwise, the performance of BLRT depends on the value of the unknown \mathbf{z}_n parameter, whereas GLRT is CFAR. Thus, the detectors are not generally equivalent. Interestingly, the next theorem shows that CLRT, with the added CFAR constraint, is equivalent to GLRT.

Theorem 2. *Consider the classical asymptotic setting with a block diagonal Fisher Information Matrix (FIM) and the technical assumptions detailed in the appendix. Then, independently of the choice of $p(\mathbf{z})$ prior, CLRT is equivalent to GLRT, that is, GLRT is a solution to (14).*

Sketch of proof of Theorem 1: We provide the main ideas leaving the technical details to Appendix A. First, consider the case of nuisance parameters. Here, GLRT is defined as

$$T_{\text{GLRT}}(\mathbf{x}) = 2\log \frac{\prod_{i=1}^N p(x_i; \hat{\mathbf{z}}_r)}{\prod_{i=1}^N p(x_i; \mathbf{z}_{r_0})} \quad (19)$$

where $\hat{\mathbf{z}}$ is the ML estimator:

$$\hat{\mathbf{z}}_r = \arg \max \prod_{i=1}^N p(x_i; \mathbf{z}_r) \quad (20)$$

BLRT is defined as

$$T_{\text{BLRT}}(\mathbf{x}) = 2\log \frac{\int \prod_{i=1}^N p(x_i; \mathbf{z}_r) p(\mathbf{z}_r) d\mathbf{z}_r}{\prod_{i=1}^N p(x_i; \mathbf{z}_{r_0})} \quad (21)$$

Laplace's approximation [36–39] for the integral yields

$$\int \prod_{i=1}^N p(x_i; \mathbf{z}_r) p(\mathbf{z}_r) d\mathbf{z}_r \rightarrow \prod_{i=1}^N p(x_i; \hat{\mathbf{z}}_r^J) p(\hat{\mathbf{z}}_r^J) \text{func}(\hat{\mathbf{z}}_r^J) \quad (22)$$

where

$$\hat{\mathbf{z}}_r^J = \arg \max_{\mathbf{z}_r} \prod_{i=1}^N p(x_i; \mathbf{z}_r) p(\mathbf{z}_r) d\mathbf{z}_r. \quad (23)$$

Note that this estimate is also the maximum a posteriori (MAP). Thus BLRT converges to:

$$T_{\text{BLRT}}(\mathbf{x}) = \frac{1}{2} \sum_{i=1}^N \log \frac{p(x_i, \hat{\mathbf{z}}_r^J)}{p(x_i, \mathbf{z}_{r_0})} + \text{func}(\hat{\mathbf{z}}_r^J) \quad (24)$$

Comparing the two detectors reveals two differences which vanish asymptotically (see the appendix for the exact analysis with convergence rates):

- GLRT involves the maximum of the likelihood $\hat{\mathbf{z}}$ whereas BLRT uses the the maximum of the joint distribution $\hat{\mathbf{z}}^J$. Fortunately, the difference is asymptotically negligible as only the log likelihood scales with N :

$$\hat{\mathbf{z}}_r^J \rightarrow \hat{\mathbf{z}}_r \quad (25)$$

- BLRT involves an additional function of $\hat{\mathbf{z}}_r^J$ which depends on the random \mathbf{x} and may change its performance. Here too the asymptotic regime comes to the rescue and we rely on consistency of the MLE and the weak signal assumption:

$$\mathbf{z}_r^J \rightarrow \hat{\mathbf{z}}_r \rightarrow \mathbf{z}_{r_0/1} \approx \mathbf{z}_{r_0} \quad (26)$$

so that, asymptotically, the function depends on a known value.

In case of nuisance parameters, the analysis is similar. The only difference is that GLRT uses maximizations on both hypotheses (in the nominator and in the denominator), whereas BLRT requires integral approximations in both. Following the same steps as before yields

$$T_{\text{GLRT}}(\mathbf{x}) = 2\log \frac{\prod_{i=1}^N p(x_i; \hat{\mathbf{z}})}{\prod_{i=1}^N p(x_i; \mathbf{z}_{r_0}, \hat{\mathbf{z}}_{n_0})}$$

$$T_{\text{BLRT}}(\mathbf{x}) = 2\log \frac{\prod_{i=1}^N p(x_i; \hat{\mathbf{z}})}{\prod_{i=1}^N p(x_i; \mathbf{z}_{r_0}, \hat{\mathbf{z}}_{n_0})} + \text{func}(\mathbf{z}_{r_0}, \mathbf{z}_n), \quad (27)$$

where $\hat{\mathbf{z}}_{n_0}$ is the constrained MLE such that $\mathbf{z}_r = \mathbf{z}_{r_0}$.

Proof of Theorem 2: GLRT is asymptotically CFAR and if the FIM is block diagonal its performance with unknown nuisance parameters is the same as if they where known (see Appendix C). Thus, GLRT has the best expected (over \mathbf{z}_r) TPR for any given FPR, for any \mathbf{z}_n . Now, we write the Bayes risk as the sum of the expected FPR and the expected false negative rate (FNR, which is 1-TPR): Given a test $(T(\mathbf{x}), \gamma)$, we denote the expected FPR for a given \mathbf{z}_n by:

$$\alpha(T, \gamma, \mathbf{z}_n) = \Pr(T(\mathbf{x}) > \gamma | y = 0, \mathbf{z}_n), \quad (28)$$

and similarly the expected FNR for a given \mathbf{z}_n by:

$$\beta(T, \gamma, \mathbf{z}_n) = \Pr(T(\mathbf{x}) < \gamma | y = 1, \mathbf{z}_n). \quad (29)$$

The objective of CLRT is therefore:

$$L_{0-1}(T, \gamma) = p_0 \Pr[\alpha(T, \gamma, \mathbf{z}_n)] + p_1 \Pr[\beta(T, \gamma, \mathbf{z}_n)], \quad (30)$$

where the expectations are over $p^{\text{fake}}(\mathbf{z}_n)$.

We now show that the GLRT with some threshold γ , is a solution to (14) which can be written as:

$$\begin{aligned} \min_{T(\mathbf{x}), \gamma} \quad & L_{0-1}(T, \gamma) \\ \text{s.t.} \quad & \alpha(T, \tilde{\gamma}, \mathbf{z}_n) = \alpha(T, \tilde{\gamma}, \mathbf{z}'_n) \quad \forall \mathbf{z}_n, \mathbf{z}'_n, \tilde{\gamma}, \end{aligned} \quad (31)$$

Note that the constraint must be satisfied for all $\tilde{\gamma}$ and not just for the optimal γ .

Due to the CFAR constraint, the FPR is constant with respect to \mathbf{z}_n and so is its expectation:

$$\mathbb{E}[\alpha(T, \gamma, \mathbf{z}_n)] = \alpha(T, \gamma), \quad (32)$$

where $\alpha(T, \gamma)$ is the FPR of the test on any value of \mathbf{z}_n . Thus the Bayesian 0-1 loss can be written as:

$$L_{0-1}(T, \gamma) = p_0 \alpha(T, \gamma) + p_1 \mathbb{E}[\beta(T, \gamma, \mathbf{z}_n)]. \quad (33)$$

The best threshold for any detector can be therefore found by minimizing (33) with respect to γ . Specifically we denote the optimal threshold of the GLRT detector by γ^* , and denote the corresponding FPR as α^* .

Now we prove that any other CFAR detector gives a larger or equal Bayesian 0-1 loss. We assume that there exist a detector $(T'(\mathbf{x}, \mathbf{z}_n), \gamma')$ that has FPR of α' for any value of \mathbf{z}_n . Its Bayesian loss is given by:

$$\begin{aligned} L_{0-1}(T', \gamma') &= p_0 \alpha' + p_1 \mathbb{E}[\beta(T', \gamma', \mathbf{z}_n)] \\ &\geq p_0 \alpha' + p_1 \mathbb{E}[\beta(T_{\text{GLRT}}, \gamma'_{\text{GLRT}}, \mathbf{z}_n)] \\ &= L_{0-1}(T_{\text{GLRT}}, \gamma'_{\text{GLRT}}) \\ &\geq L_{0-1}(T_{\text{GLRT}}, \gamma^*), \end{aligned} \quad (34)$$

where γ'_{GLRT} is the threshold that gives FPR of α' to the GLRT. The first inequality is due to the optimality of GLRT among detectors that have FPR α' for any value of \mathbf{z}_n . The second inequality is due to the optimality of the threshold γ^* for the GLRT detector.

In conclusion, the GLRT with threshold γ^* gives the minimum Bayesian loss among all the detectors that have constant false alarm rate over \mathbf{z}_n . In other words, GLRT and CLRT are equivalent, completing the proof.

Returning to Example 1: To derive the Bayesian versions of the detectors, we assume a fictitious prior $A \sim \mathcal{N}(0, \sigma_r^2)$. If the noise variance σ^2 is known (no nuisance parameters), then BLRT is given by

$$T_{\text{BLRT}}(\mathbf{x}) = \frac{(\mathbf{x}^T \mathbf{1})^2}{N\sigma^2 + \sigma_r^2} + \log\left(\frac{\sigma^2}{\sigma^2 + N\sigma_r^2}\right) \quad (35)$$

The variances are all known and appropriate thresholds can be selected so that BLRT and GLRT in (9) are asymptotically equivalent.

On the other hand, if σ^2 unknown then BLRT is more complicated and does not satisfy a simple closed form solution. Yet, independently of the chosen prior for σ^2 ,

its limit can be derived as

$$T_{\text{BLRT}}(\mathbf{x}) \xrightarrow{N \rightarrow \infty} \frac{(\mathbf{x}^T \mathbf{1})^2}{\mathbf{x}^T \mathbf{x}} + \log\left(\frac{\mathbf{x}^T \mathbf{x}}{N^2 \sigma_r^2}\right). \quad (36)$$

Evidently, this asymptotic BLRT and the GLRT in (10) are not equivalent. Their ROC performance are similar as $\mathbf{x}^T \mathbf{x} \rightarrow N\sigma^2$ but BLRT requires different thresholds and does not have a CFAR.

V. LEARNED DETECTORS

A. Background and existing work

In this section, we propose a framework for learning neural networks that approximate the theoretical Bayesian detectors. Historically, Bayesian detectors were considered intractable due to the required high dimensional integration. This changed with the recent deep learning revolution. The latter are in fact data-driven Bayesian detectors. The differences are that the Bayesian probabilities and expectations are replaced by empirical averages with respect to a training set and that the optimizations are restricted to a class of neural networks. The resulting networks provide practical alternatives to the classical detectors in terms of both accuracy and computational complexity.

The starting point to machine learning is data. In the simplest setting, the training dataset is synthetic and consists of artificial samples. The dataset is generated using the (possibly fictitious) priors $\Pr(y)$, $p(\mathbf{z}; y)$ and the probabilistic model $p(\mathbf{x}; \mathbf{z})$. That is, first y and \mathbf{z} are generated according to their priors. For each $y^{(k)}$ and $\mathbf{z}^{(k)}$, a measurement $\mathbf{x}^{(k)}$ is generated according to the true $p(\mathbf{x}; \mathbf{z}^{(k)})$. Together, we obtain a synthetic dataset:

$$\mathcal{D}_N = \{\mathbf{x}^{(k)}, \mathbf{z}^{(k)}, y^{(k)}\}_{k=1}^K. \quad (37)$$

In more advanced settings, there are also hybrid datasets involving a mixture of real and artificial samples. For example, it is standard to plant synthetic targets on real noise or clutter samples [11].

Next, a class of possible detectors \mathcal{T} is chosen in order to tradeoff expressive power with computational complexity in test time. The class is usually a fixed differentiable neural network architecture. In our context, it also makes sense to reuse existing ingredients from classical detector as non-linear features or internal sub-blocks [7, 23].

Finally, the learned detector is defined as the minimizer of an empirical loss function

$$\min_{\hat{T} \in \mathcal{T}} \frac{1}{K} \sum_{k=1}^K L(\hat{T}(\mathbf{x}^{(k)}), y^{(k)}). \quad (38)$$

where $L(\cdot; \cdot)$ is a classification loss function. Ideally, we would like to minimize the zero-one loss which corresponds to the average probability of error. Practically, for efficient optimization, a smooth and convex surrogate loss, as the hinge or cross entropy functions, is preferable. The overall procedure for learning a detector is summarized in Algorithm 1.

Algorithm 1 Bnet: learning an approximation to BLRT.

- Require $p(\mathbf{x}; \mathbf{z})$.
- Choose $\Pr(y)$ and $p(\mathbf{z}; y)$.
- For each $k = 1, \dots, K$:
 - Generate $y^{(k)}$.
 - Generate $\mathbf{z}^{(k)}$ given $y^{(k)}$.
 - Generate $\mathbf{x}^{(k)}$ given $\mathbf{z}^{(k)}$.
- Solve

$$\min_{\hat{T} \in \mathcal{T}} \frac{1}{K} \sum_{k=1}^K L(\hat{T}(\mathbf{x}^{(k)}), y^{(k)}).$$

Learned detectors can efficiently approximate any required BLRT. This requires a large enough training dataset, an expressive enough class of possible detectors \mathcal{T} and a Bayes risk consistent surrogates, as the hinge loss [40]. When the hypotheses are simple, such solutions are also optimal in the classical sense.

B. CFARnet

We now show that CLRT can also be approximated using a neural network denoted by CFARnet. Like Bnet, the approximation will be accurate if the training dataset is large enough and the class of detectors is expressive enough. The only difference in CFARnet is the introduction of an additional differentiable CFAR penalty which approximates the constraint. The rest of this subsection provides its details.

To approximate the CFAR constraint CFARnet introduces two modifications to Algorithm 1. First, we augment the classification loss with a penalty function that ensures similar distributions of the detector $\hat{T}(\mathbf{x})$ for all values of $\mathbf{z} \in \mathcal{H}_0$. Second, in order to compare such distributions empirically, we rely on an enhanced training set that includes multiple $\{\mathbf{x}^{(k,m)}\}_{m=1}^M$ for each $\mathbf{z}^{(k)}$.

The main idea is adding a penalty to the objective function that promotes a CFAR detector. For this purpose, we need to measure the distance between different distributions.

Definition 2. Let $X \sim p(X)$ and $Y \sim p(Y)$ be two random variables. A statistical distance $d(X; Y)$ is a function that satisfies $d(X; Y) \geq 0$ with equality if and only if $p(X) = p(Y)$. In particular, a statistical distance $d(X; Y)$ can be empirically estimated using a set of data realizations $\hat{d}(\{X^{(m)}\}_{m=1}^M, \{Y^{(m)}\}_{m=1}^M)$.

Given a statistical distance $d(\cdot; \cdot)$, the penalty is defined as a sum of distances between the distributions of \hat{T} under different values of \mathbf{z} :

$$R(\hat{T}) = \sum_{\mathbf{z}, \mathbf{z}' \in \mathcal{Z}_0} d(\hat{T}(\mathbf{x}); \hat{T}(\mathbf{x}')) \quad (39)$$

where

$$\begin{aligned} \mathbf{x} &\sim p(\mathbf{x}; \mathbf{z}) \\ \mathbf{x}' &\sim p(\mathbf{x}; \mathbf{z}'). \end{aligned} \quad (40)$$

Clearly, any CFAR test must satisfy $R(\hat{T}) = 0$.

Practically, to minimize (39), we use empirical estimates of the distances where each distribution is represented using a

small dataset. For each $\mathbf{z}^{(k)}$, we synthetically generate multiple observations $\mathbf{x}^{(k,m)}$ for $m = 1, \dots, M$. Similarly, for each $\mathbf{z}^{(k')}$ we compute multiple $\mathbf{x}^{(k',m)}$. We then plug these into the empirical distances:

$$\hat{R}(\hat{T}) = \sum_{\substack{k : y^{(k)} = 0 \\ k' : y^{(k')} = 0}} \hat{d} \left(\{\hat{T}(\mathbf{x}^{(k,m)})\}_{m=1}^M; \{\hat{T}(\mathbf{x}^{(k',m)})\}_{m=1}^M \right) \quad (41)$$

where the sum is only computed with respect to samples corresponding to $y = 0$.

Our implementation of CFARnet uses the Maximum Mean Discrepancy (MMD) distance [26] as detailed in Appendix D. We also use a hyper-parameter $\alpha > 0$ that trades off the importance of the classification accuracy versus the CFAR penalty. The overall CFARnet procedure is summarized in Algorithm 2.

Algorithm 2 CFARnet: learning an approximation to CLRT

- Require $p(\mathbf{x}; \mathbf{z})$.
- Choose $\Pr^{\text{fake}}(y)$ and $p^{\text{fake}}(\mathbf{z}; y)$.
- For each $k = 1, \dots, K$:
 - Generate $y^{(k)}$.
 - Generate $\mathbf{z}^{(k)}$ given $y^{(k)}$.
 - For $m = 1, \dots, M$:
 - Generate $\mathbf{x}^{(k,m)}$ given $\mathbf{z}^{(k)}$.
- Solve

$$\min_{\hat{T} \in \mathcal{T}} \frac{1}{KM} \sum_{k,m} L(\hat{T}(\mathbf{x}^{(k,m)}), y^{(k)}) + \alpha \hat{R}(\hat{T}).$$

VI. NUMERICAL EXPERIMENTS

In this section, we demonstrate the advantages of CFARnet via numerical experiments. In all our experiments we evaluate Bnet, which is a standard learned neural network (Algorithm 1), CFARnet (algorithm 2) and in the first two experiments, one or more classical methods. Bnet and CFARnet have identical architecture and both of them are trained using stochastic optimization [41], until the loss function reaches a plateau. The classification loss for Bnet and CFARnet is cross-entropy and the CFAR penalty for CFARnet is MMD. We choose the parameter α such that the two losses are of comparable values. Empirically we found that increasing α more, does not improve much the level of CFARness, however we did not focus on this analysis. Full implementation details are provided in the Supplementary Material.

A. Signal in uncorrelated noise

In our first experiment, we consider the running Example 1 of unknown target amplitude and unknown noise scaling as defined in (2)-(3). We compare three detectors:

- GLRT: Assuming Gaussian noise, the classical GLRT has a simple closed form solution (10) and is known to be CFAR.
- Bnet: A learned neural network as in Algorithm 1. We choose a uniform fake prior for the unknown parameters

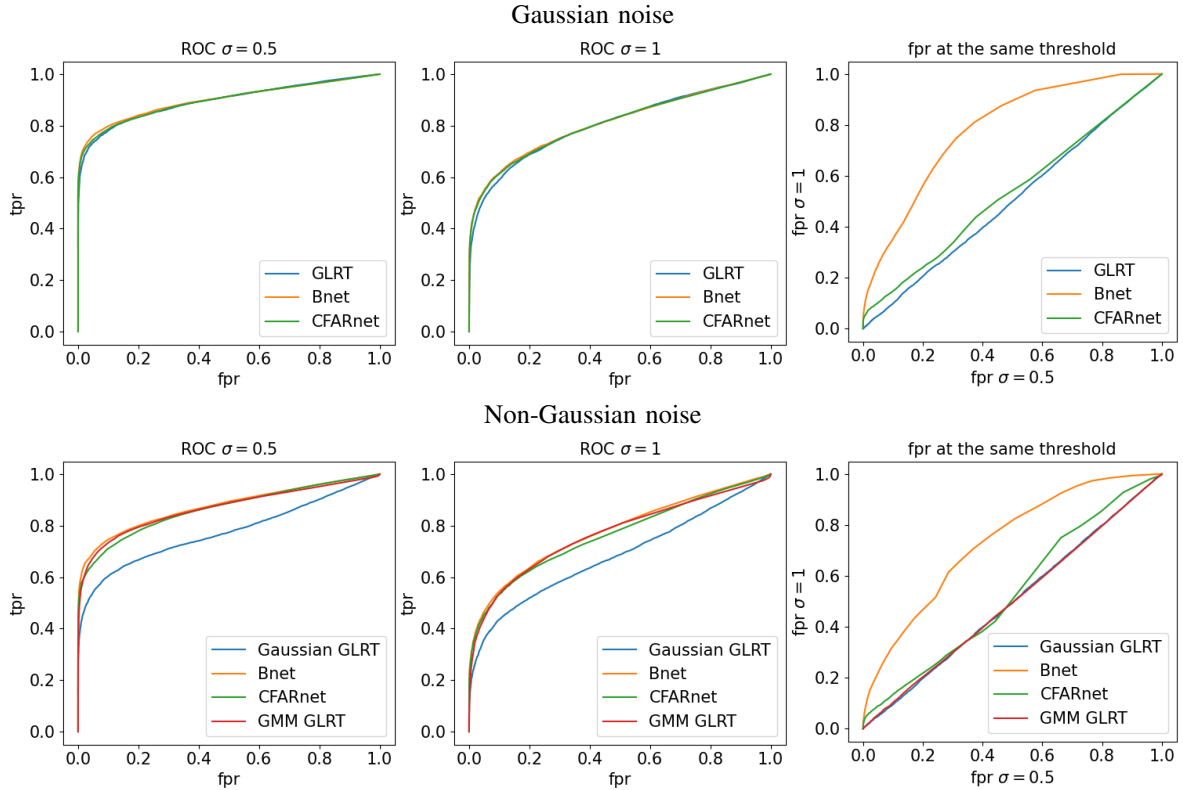


Fig. 1. Results of the uncorrelated noise experiment. Performance graphs in terms of FPR, TPR and thresholds for different values of the nuisance parameter σ . The left and the middle columns show the ROC curve for $\sigma = 0.5$ and $\sigma = 1$. The right column shows the FPR at $\sigma = 0.5$ vs. $\sigma = 1$. Note that a CFAR detector results in a diagonal line. The top row is with Gaussian noise and indeed the Gaussian GLRT is best both in terms of ROC and CFAR. Bnet succeeds in achieving its ROC but is not CFAR. CFARnet is both accurate and CFAR. Bottom row is with non-Gaussian noise and the learned detectors beat the Gaussian GLRT in accuracy. CFARnet is near CFAR with a slight decrease in accuracy, but again is approximately CFAR.

in (3). The architecture is based on four non-linear features: the sample mean of \mathbf{x} , its sample variance and robust versions of the two based on the median. These features are passed through a fully connected neural network

- CFARnet: A learned neural network as in Algorithm 2 with CFAR penalty parameter $\alpha = 1$.

The prior of A and σ that was used for generating the training data for Bnet and CFARnet is uniform distribution in the following region:

$$-1 \leq A \leq 1, \quad 0.5 \leq \sigma \leq 1. \quad (42)$$

The first experiment considers Gaussian noise. In the first row of Fig. 1, we plot the two ROCs for different values of σ . To examine the CFAR property, we also plot the FPRs under different parameters. As expected, it is easy to see that the Gaussian GLRT performs well and is CFAR. Bnet provides similar accuracy as illustrated in its ROC but is non-CFAR. It results in significantly different FPR when we change σ . On the other hand, CFARnet is both accurate and near CFAR.

The next setup is more challenging and considers non-Gaussian noise. The setting is identical to Example 1 except for the noise distribution which is modified to

$$p(n_i) = (1 - \epsilon)\mathcal{N}(0, 1) + \epsilon\mathcal{N}(0, 100) \quad (43)$$

where $\epsilon = 0.1$. This setting represents a Gaussian noise with outliers.

Here we add a more advanced detector, GMM GLRT, which is the GLRT associated with the true noise distribution, where the optimizations are performed using the common Expectation-Maximization algorithm [42]. The results are provided in the second row of Fig. 1. In this case, the Gaussian GLRT is no longer optimal and the two learned detectors provide a significantly better ROC and with similar results to the GMM GLRT. In terms of CFAR, GLRT is still invariant to the nuisance parameter, but the FPR of Bnet is dependent on its value. As argued, CFARnet is both accurate and CFAR. Finally we compare the inference time of the algorithms. Table C shows the AUC and inference time on test set of 20000 samples, in milliseconds. CFARnet and GMM GLRT have similar AUC and are much better than Gaussian GLRT, but CFARnet is almost 8 times faster than GMM GLRT.

B. Gaussian signal in correlated noise

In our second experiment, we consider the detection of a known signal \mathbf{s} with unknown amplitude in Gaussian noise with unknown covariance Σ . This is a classical problem in adaptive target detection [27, 28]. Following these works, we

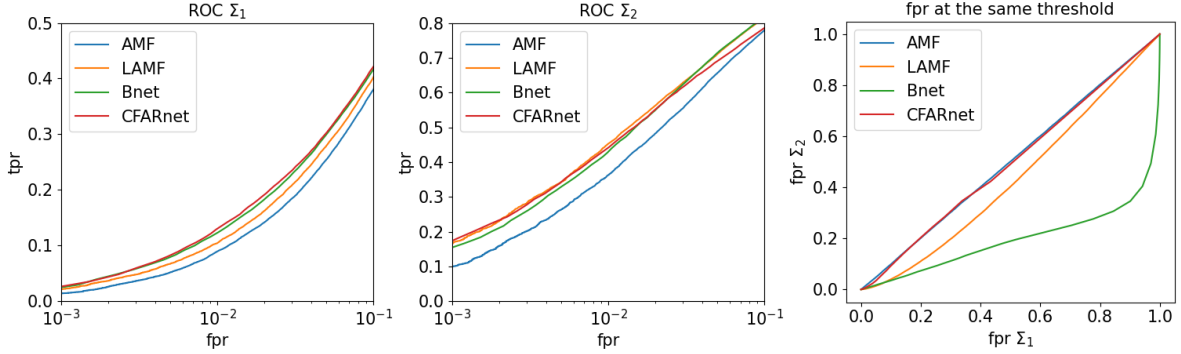


Fig. 2. Results of the correlated noise experiment. Performance graphs in terms of FPR, TPR and thresholds for two different values of Σ . LAMF, Bnet and CFARnet are better than AMF (especially at the interesting low-FPR regime). Unlike CFARnet, the LAMF and Bnet are highly non-CFAR.

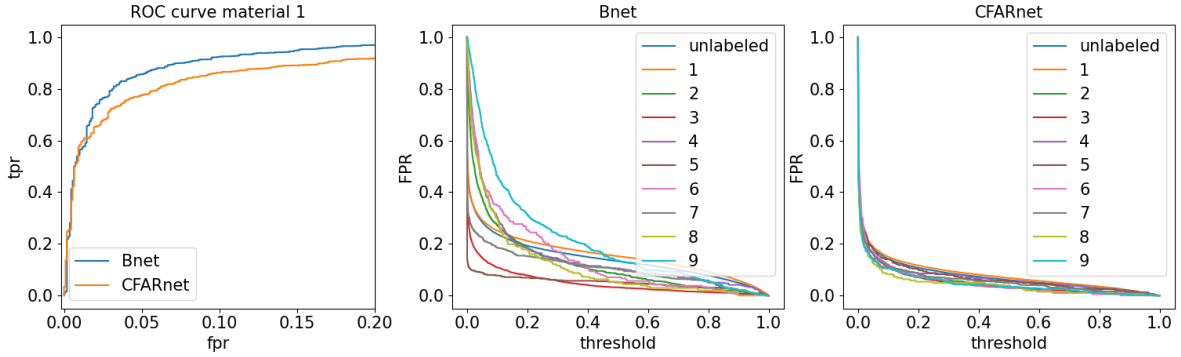


Fig. 3. Experiment C. Performance graphs in terms of FPR, TPR and threshold. The left plot shows the ROC curve for one of the materials. The two right plots shows the FPR as a function of the threshold for each material. While Bnet is better in terms of ROC curve, it is far from CFAR, while CFARnet is approximately CFAR.

TABLE I
AUC AND INFERENCE TIME IN THE UNCORRELATED NOISE EXPERIMENT

DETECTOR	AUC	INFERENCE TIME [MSEC]
GAUSSIAN GLRT	0.78	1.3
GMM GLRT	0.869	89
CFARNET	0.865	13

assume a secondary data of n i.i.d. noise-only samples $\mathbf{x}_{aux} = (\mathbf{w}_1, \dots, \mathbf{w}_n)$. Together the observations can be modelled as

$$\begin{aligned} \mathbf{x} &= A\mathbf{s} + \mathbf{w}_0 \\ \mathbf{x}_i &= \mathbf{w}_i \quad i = 1, \dots, n \end{aligned} \quad (44)$$

where

$$\mathbf{w}_0, \mathbf{w}_i \sim \mathcal{N}(\mathbf{0}, \Sigma) \quad (45)$$

In terms of the standard notations of detection from earlier, The vector \mathbf{z} includes both A and all the elements in the matrix Σ . The goal is to decide between

$$\begin{aligned} y = 0 : \quad A &= 0 \\ y = 1 : \quad A &\neq 0. \end{aligned} \quad (46)$$

The classical adaptive matched filter (AMF) detector is given by: [28]:

$$T_{AMF}(\mathbf{x}) = \frac{(\mathbf{s}^T \hat{\Sigma}^{-1} \mathbf{x})^2}{\mathbf{s}^T \hat{\Sigma}^{-1} \mathbf{s}} \quad (47)$$

with

$$\hat{\Sigma} = \frac{1}{n} \sum_{i=1}^n \mathbf{w}_i \mathbf{w}_i^T. \quad (48)$$

The AMF in (47) is CFAR but is sub-optimal when n is small. In such settings, it is common to plug in regularized covariance estimators:

$$\hat{\Sigma}_\lambda = \hat{\Sigma} + \lambda \mathbf{I}. \quad (49)$$

This leads to the popular diagonally loaded LAMF which is generally not CFAR [31, 32].

To design a CFAR version of the above detectors, we train a simple model of fully connected network with a single hidden layer, with the following features as inputs:

$$\begin{aligned} f_1^\lambda(\mathbf{x}) &= \mathbf{s}^T \hat{\Sigma}_\lambda^{-1} \mathbf{x} \\ f_2^\lambda(\mathbf{x}) &= \mathbf{s}^T \hat{\Sigma}_\lambda^{-1} \mathbf{s} \\ f_3^\lambda(\mathbf{x}) &= \mathbf{x}^T \hat{\Sigma}_\lambda^{-1} \mathbf{x}. \end{aligned} \quad (50)$$

We use 10 different linearly spaced values of λ between 0 and 0.3. The input to the neural network in this case is a concatenation of all 30 features to a single vector. The parameter α is set to be 0.5. Fig. 2 shows the ROC curves of AMF, LAMF with $\lambda = 0.03$, Bnet and CFARnet on two different covariances. We also plot the FPRs under different parameters. The performance of LAMF, Bnet and CFARnet are better than AMF (especially at the interesting low-FPR regime). While LAMF and Bnet are far from CFAR, CFARnet is approximately CFAR.

C. Target detection in real-world hyperspectral image

The main motivation to CFARnet is training detectors using a synthetic dataset with continuous large scale parameters. For completeness, however, our last experiment considers the use of CFARnet in a (semi) real world setting with a finite valued nuisance parameter. Specifically, we consider target detection in real hyperspectral images annotated according to a finite number of materials. The image is taken from the Pavia University dataset. Fifth of the pixels are annotated to be one of nine materials, e.g., asphalt or trees. We use these annotations as the unknown \mathbf{z} parameters. Following [11], we synthetically plant artificial targets on the real image. The target's spectrum is taken from the USGS Spectral Library [14] and is interpolated to fit the 103 bands of the hyperspectral image. It is planted randomly (with probability of a half) in the image using an additive model:

$$\mathbf{x} = \alpha \mathbf{t} + \mathbf{v} \quad (51)$$

where \mathbf{v} is the original pixel vector, \mathbf{t} is the target and $\alpha = 0.05$ is the amplitude of the target. For simplicity, the distribution of the targets is known and the only unknown parameter is the background material. The image contains about 210000 pixels and we use two thirds of the image for training and the rest for testing (each pixel is treated independently). Note that the unrealistic density of targets is not an issue as we evaluate on classical metrics where the labels are deterministic unknown.

We train a simple fully-connected neural network with two hidden layers of size 100. First, we fit Bnet using a standard cross entropy loss and then using CFARnet. To overcome the imbalance between the number of examples of each material, in each step of the stochastic gradient descent, we randomly choose one material and generate a batch for it. Fig. 3 shows that while Bnet is better in terms of ROC curve, it is far from CFAR. CFARnet shows an expected degradation in performance but is approximately CFAR. To get additional insight on the price of CFAR, we also consider a natural baseline that uses Bnet but computes its threshold to guarantee a required FPR constraint on the worst case material. Table II compares the partial AUC of the TPR as a function of the worst case FPR in (0–0.05). It can be seen that in all materials except the unlabeled, CFARnet is better with respect to this metric.

TABLE II
PARTIAL AUC IN (0 – 0.05) OF TPR AS A FUNCTION OF THE WORST CASE FPR.

MATERIAL	BNET	CFARNET
UNLABELED	0.49	0.47
1	0.31	0.38
2	0.74	0.77
3	0.33	0.35
4	0.69	0.73
5	0.27	0.34
6	0.49	0.53
7	0.47	0.72
8	0.41	0.49
9	0.88	0.9

VII. DISCUSSION AND FUTURE WORK

In recent years, deep neural networks are become popular and are used for detection problems in many fields. While deep learning based detectors give remarkable improvements in accuracy, they are not CFAR and are thus unsuitable in many practical settings. We thus propose a method to train a deep learning detector that is CFAR, prove that it converges to GLRT in asymptotic settings, and show empirically that it results in CFAR detectors with a minor decrease in performance, on both synthetic and real data. It is important to address the limitations of the proposed framework. Fundamentally, our results demonstrate the asymptotic advantages of CFAR, but in finite samples there is an inherent tradeoff between fairness and accuracy that cannot be avoided. On the technical side, our implementation of CFARnet assumes that the synthetic dataset can be generated with full control of the parameters in the model, or using real datasets that are annotated according to the value of their nuisance parameters. Future work can focus on relaxing these assumptions as well as evaluating the method in larger and more realistic settings.

ACKNOWLEDGMENT

The authors would like to thank Yoav Wald for fruitful discussions and helpful insights. This research was partially supported by ISF grant number 2672/21.

APPENDIX

A. Details and full proof of Theorem 1

We begin by clearly specifying all the needed technical assumptions denoted by (Ax):

- (A1) The input consists of N i.i.d samples from $p(\mathbf{x}; \mathbf{z})$.
- (A2) Weak signal: under the $y = 1$ hypothesis, the true parameter \mathbf{z}_{r_1} satisfies $\|\mathbf{z}_{r_1} - \mathbf{z}_{r_0}\| = s/\sqrt{N}$ where $s > 0$ is a constant.
- (A3) The MLE converges to its asymptotic form [43]:

$$\sqrt{N} \hat{\mathbf{z}} \sim \mathcal{N} \left(\mathbf{z}, \mathcal{I}^{-1} \right), \quad (52)$$

where \mathcal{I} is the Fisher Information Matrix (FIM)¹

$$\mathcal{I} = \mathbb{E} \left[\frac{\partial^2 \log(p(x; \mathbf{z}))}{\partial \mathbf{z}^2} \right] = \begin{pmatrix} \mathcal{I}_{rr} & \mathcal{I}_{rn} \\ \mathcal{I}_{rn}^T & \mathcal{I}_{nn} \end{pmatrix}. \quad (53)$$

- (A4) The FIM \mathcal{I} is not singular at the true parameter.
- (A5) The FIM is block diagonal, i.e., $\mathcal{I}_{rn} = \mathbf{0}$.
- (A6) The priors $p(\mathbf{z}_r)$ and $p(\mathbf{z}_n)$ are not zero at \mathbf{z}_{r_0} and do not depend on N .
- (A7) The standard regularity conditions needed for Laplace approximation for marginal distribution as detailed in [44] (see page 26-27 there). As explained there, these are standard asymptotically assumptions. Note also that some of them are related to the assumptions that we already stated, but we give them explicitly as we need them not only for the Laplace approximation.

Note that most of these assumptions are technical and standard, and follow [16] and [44]. The only non trivial assumption is (A5). It is satisfied in many classical models, e.g., in Gaussian distribution when the amplitude of the signal depend on the discriminative parameters and the covariance depends on the nuisance parameters. Future work may focus on relaxing this assumption.

Under assumptions A1-A7, the following limits hold in probability tending to one when $N \rightarrow \infty$:

- (B1) The MLE converges to the true parameter:

$$\hat{\mathbf{z}} = \mathbf{z} + O\left(\frac{1}{\sqrt{N}}\right) \quad (54)$$

Proof: (A3).

- (B2) The log likelihood at the MAP and the log likelihood at the MLE are related by:

$$\sum_{i=1}^N p(x_i; \hat{\mathbf{z}}_r^J) = \sum_{i=1}^N p(x_i; \hat{\mathbf{z}}) + O\left(\frac{1}{N}\right), \quad (55)$$

Proof: Appendix B.

- (B3) The marginal distribution can be computed using Laplace's approximation:

$$p_1(\mathbf{x}) = \tilde{p}_1(\mathbf{x}) \left(1 + O\left(\frac{1}{N}\right)\right). \quad (56)$$

where $p_1(\mathbf{x})$ is the exact marginal density:

$$p_1(\mathbf{x}) = \int \prod_{i=1}^N p(x_i; \mathbf{z}) p(\mathbf{z}) d\mathbf{z}, \quad (57)$$

and $\tilde{p}_1(\mathbf{x})$ is the Laplace approximated density:

$$\tilde{p}_1(\mathbf{x}) = \prod_{i=1}^N p(x_i; \hat{\mathbf{z}}_r^J) p(\hat{\mathbf{z}}_r^J) \sqrt{\frac{(2\pi)^{d_r}}{N^{d_r} \det(\tilde{\mathcal{I}}(\hat{\mathbf{z}}_r^J))}}, \quad (58)$$

where

$$\tilde{\mathcal{I}} = \frac{1}{N} \sum_{i=1}^N \frac{\partial^2 \log(p(x_i; \mathbf{z}))}{\partial \mathbf{z}^2} \quad (59)$$

¹Note the difference of our notation from [16] where the joint $p(\mathbf{x}; \mathbf{z})$ is used, compared to our definition where we use the FIM of a the single sample distribution $p(x; \mathbf{z})$.

is the Hessian.

Proof: (A7) and [44, 45].

- (B4) The Hessian converges to the FIM: $\tilde{\mathcal{I}} \rightarrow \mathcal{I}$ and thus for large enough N , the Hessian is not singular (by A4).

Proof: weak law of large numbers.

Given these limits, we turn to proving Theorem 1. We start with the case of no nuisance parameters. GLRT (19) and BLRT (21) can be written as

$$T_{\text{GLRT}}(\mathbf{x}) = 2 \sum_{i=1}^N \log(p(x_i; \hat{\mathbf{z}}_r)) - 2 \sum_{i=1}^N \log(p(x_i; \mathbf{z}_{r_0})) \quad (60)$$

$$T_{\text{BLRT}}(\mathbf{x}) = 2 \log \int \prod_{i=1}^N p(x_i; \mathbf{z}_r) p(\mathbf{z}_r) d\mathbf{z}_r - 2 \sum_{i=1}^N \log(p(x_i; \mathbf{z}_{r_0})) \quad (61)$$

Taking the log of the marginal after Laplace approximation (56) gives:

$$\begin{aligned} \log(p_1(\mathbf{x})) &= \log \int \prod_{i=1}^N p(x_i; \mathbf{z}_r) p(\mathbf{z}_r) d\mathbf{z}_r \\ &= \sum_{i=1}^N \log(p(x_i; \hat{\mathbf{z}}_r^J)) + \log(p(\hat{\mathbf{z}}_r^J)) \\ &\quad + \frac{1}{2} d_r \log\left(\frac{2\pi}{N}\right) - \frac{1}{2} \log\left(\det(\tilde{\mathcal{I}}(\hat{\mathbf{z}}_r^J))\right) \\ &\quad + \log\left(1 + O\left(\frac{1}{N}\right)\right) \end{aligned} \quad (62)$$

Now we use (B2) and plug (55) into (62) and then to 61. In addition we use:

$$\log\left(1 + O\left(\frac{1}{N}\right)\right) = O\left(\frac{1}{N}\right), \quad (63)$$

and get:

$$\begin{aligned} T_{\text{BLRT}} &= 2 \sum_{i=1}^N \log(p(x_i; \hat{\mathbf{z}}_r)) - 2 \sum_{i=1}^N \log(p(x_i; \mathbf{z}_{r_0})) \\ &\quad + d_r \log\left(\frac{2\pi}{N}\right) + 2 \log(p(\hat{\mathbf{z}}_r^J)) \\ &\quad - \log\left(\det(\tilde{\mathcal{I}}(\hat{\mathbf{z}}_r^J))\right) + O\left(\frac{1}{N}\right). \end{aligned} \quad (64)$$

The first two terms are exactly the GLRT.

Next, we use Taylor theorem to approximate the terms that depend on $\hat{\mathbf{z}}_r$ and $\hat{\mathbf{z}}_r^J$ by their values at \mathbf{z}_0 . For any close enough \mathbf{z}_1 and \mathbf{z}_2 , and for any two-times differentiable function q we have that:

$$q(\mathbf{z}_2) = q(\mathbf{z}_1) + O(\|\mathbf{z}_2 - \mathbf{z}_1\|) \quad (65)$$

Using (A2) and (B1)-(B2) yield

$$\begin{aligned} \hat{\mathbf{z}}_r &= \mathbf{z}_{r_0} + O\left(\frac{1}{\sqrt{N}}\right) \\ \hat{\mathbf{z}}_r^J &= \mathbf{z}_{r_0} + O\left(\frac{1}{\sqrt{N}}\right). \end{aligned} \quad (66)$$

Plugging (66) into (65) together with (A4) and (A6) gives:

$$\begin{aligned} \log \left(\det \left(\tilde{\mathcal{I}}(\hat{\mathbf{z}}_r) \right) \right) &= \log \left(\det \left(\tilde{\mathcal{I}}(\mathbf{z}_{r_0}) \right) \right) + O \left(\frac{1}{\sqrt{N}} \right) \\ 2 \log \left(p(\hat{\mathbf{z}}_r^J) \right) &= 2 \log \left(p(\mathbf{z}_{r_0}) \right) + O \left(\frac{1}{\sqrt{N}} \right) \end{aligned} \quad (67)$$

under both $y = 0$ and $y = 1$. Plugging these into (64) gives:

$$\begin{aligned} T_{BLRT} &= T_{GLRT} + d_r \log \left(\frac{2\pi}{N} \right) + 2 \log \left(p(\mathbf{z}_{r_0}) \right) \\ &\quad - \log \left(\det \left(\tilde{\mathcal{I}}(\mathbf{z}_{r_0}) \right) \right) + O \left(\frac{1}{\sqrt{N}} \right). \end{aligned} \quad (68)$$

Finally, because \mathbf{z}_{r_0} is known, we get that

$$T_{BLRT} = T_{GLRT} + \text{const.} + O \left(\frac{1}{\sqrt{N}} \right) \quad (69)$$

The case with nuisance parameters is very similar. Here the GLRT is given by:

$$T_{GLRT} = \frac{1}{2} \frac{\log \prod_{i=1}^N p(x_i, \hat{\mathbf{z}})}{\log \prod_{i=1}^N p(x_i, \mathbf{z}_{r_0}, \hat{\mathbf{z}}_{n_0})} \quad (70)$$

where $\hat{\mathbf{z}} = (\hat{\mathbf{z}}_r, \hat{\mathbf{z}}_n)$ is the MLE and $\hat{\mathbf{z}}_{n_0}$ is the constrained MLE where $\mathbf{z}_r = \mathbf{z}_{r_0}$ and is given by [16]:

$$\hat{\mathbf{z}}_{n_0} \approx \hat{\mathbf{z}}_n + \mathcal{I}_{nn}^{-1}(\hat{\mathbf{z}}) \mathcal{I}_{nr}(\hat{\mathbf{z}}) (\hat{\mathbf{z}}_r - \mathbf{z}_{r_0}). \quad (71)$$

Thus, using B1, the unrestricted MLE of $\hat{\mathbf{z}}_n$ and the restricted MLE $\hat{\mathbf{z}}_{n_0}$ satisfy in high probability:

$$\begin{aligned} \hat{\mathbf{z}}_n &= \mathbf{z}_n + O \left(\frac{1}{\sqrt{N}} \right) \\ \hat{\mathbf{z}}_{n_0} &= \mathbf{z}_n + O \left(\frac{1}{\sqrt{N}} \right), \end{aligned} \quad (72)$$

under both $y = 0$ and $y = 1$. The BLRT is given by:

$$T_{BLRT}(\mathbf{x}) = \frac{1}{2} \log \left(\frac{\tilde{p}_1(\mathbf{x})}{\tilde{p}_0(\mathbf{x})} \right) \quad (73)$$

where

$$\begin{aligned} \tilde{p}_1(\mathbf{x}) &= \int \prod_{i=1}^N p(x_i; \mathbf{z}_r, \mathbf{z}_n) p(\mathbf{z}_r) p(\mathbf{z}_n) d\mathbf{z}_r d\mathbf{z}_n \\ \tilde{p}_0(\mathbf{x}) &= \int \prod_{i=1}^N p(x_i; \mathbf{z}_{r_0}, \mathbf{z}_n) p(\mathbf{z}_n) d\mathbf{z}_n. \end{aligned} \quad (74)$$

Using the Laplace approximation (56) for both $\tilde{p}_1(\mathbf{x})$ and $\tilde{p}_0(\mathbf{x})$, and Taylor expansions, the BLRT can be expressed as:

$$T_{BLRT}(\mathbf{x}) = T_{BLRT}(\mathbf{x}) + \rho(\mathbf{z}_{r_0}, \mathbf{z}_n) + O \left(\frac{1}{\sqrt{N}} \right) + \text{const.} \quad (75)$$

where

$$\rho(\mathbf{z}_{r_0}, \mathbf{z}_n) = \log \left(\frac{\det(\mathcal{I}(\mathbf{z}_{r_0}, \mathbf{z}_n))}{\det(\mathcal{I}_{nn}(\mathbf{z}_{r_0}, \mathbf{z}_n))} \right). \quad (76)$$

Here \mathbf{z}_n is the unknown true value of the nuisance parameter vector.

B. Proof of B2

The proof is based on the following Lemma:

Lemma 1. Let f and h be thrice differentiable functions with unique maxima such that $|h(\mathbf{z}) - f(\mathbf{z})| = O(1/N)$ for all \mathbf{z} . Assume also that the Hessian of f at its maximum is $O(1)$ and is bounded away from zero. Denote $\hat{\mathbf{z}}^f = \arg \max f(\mathbf{z})$, $\hat{\mathbf{z}}^h = \arg \max h(\mathbf{z})$, then:

$$f(\hat{\mathbf{z}}^h) = f(\hat{\mathbf{z}}^f) + O \left(\frac{1}{N^2} \right). \quad (77)$$

The Proof of Lemma 1 is based on Taylor expansion of f and h around $\hat{\mathbf{z}}$ and maximizing the expression for \mathbf{h} . The full proof is in the Supplementary Material. We apply the lemma on

$$\begin{aligned} f(\mathbf{z}) &= \frac{1}{N} \sum_{i=1}^N \log(p(x_i; \mathbf{z})) \\ h(\mathbf{z}) &= f(\mathbf{z}) + \frac{1}{N} \log(p(\mathbf{z})). \end{aligned} \quad (78)$$

The log of the prior $\log(p(\mathbf{z}))$ is $O(1)$ and thus f and h satisfy $|h(\mathbf{z}) - f(\mathbf{z})| = O(1/N)$. The second derivative of f converges in high probability to the FIM (B4) which is non zero and is $O(1)$, Thus f and g satisfy the conditions in high probability. Thus, $\hat{\mathbf{z}}$ is the maximum of $f(\mathbf{z})$, $\hat{\mathbf{z}}^J$ is the maximum of $h(\mathbf{z})$ and (55) follows and:

$$\frac{1}{N} \sum_{i=1}^N p(x_i, \hat{\mathbf{z}}^J) = \frac{1}{N} \sum_{i=1}^N p(x_i, \hat{\mathbf{z}}) + O \left(\frac{1}{N^2} \right). \quad (79)$$

Multiplying all by N gives (55), completing the proof of B2.

C. Performance of GLRT when the FIM is block-diagonal

In the proof of theorem 2, we used the property that, when the FIM is block diagonal, the performance of GLRT with unknown nuisance parameters is the same as if they were known. Here we show this property explicitly using the asymptotic distribution of GLRT. The asymptotic distribution of GLRT is [16, p. 206]:

$$T_{GLRT} \sim \begin{cases} \chi_{d_r}^2, & y = 0 \\ \chi_{d_r}^2(\lambda), & y = 1 \end{cases} \quad (80)$$

where $\chi_{d_r}^2$, is the chi-squared distribution and $\chi_{d_r}^2(\lambda)$ is the non-central chi-squared distribution. If the there are no nuisance parameters, the parameter λ is:

$$\lambda_{\text{known}} = N(\mathbf{z}_r - \mathbf{z}_{r_0})^T \mathcal{I}(\mathbf{z}_{r_0}, \mathbf{z}_n) (\mathbf{z}_r - \mathbf{z}_{r_0}). \quad (81)$$

where \mathbf{z}_n are the known parameters of the distribution (usually the FIM is not written as a function the known parameters, but here we write this dependence explicitly to compare it to the unkown case).

If there are unknown nuisance parameters, the parameter is:

$$\begin{aligned} \lambda_{\text{unknown}} &= N(\mathbf{z}_r - \mathbf{z}_{r_0})^T (\mathcal{I}_{rr}(\mathbf{z}_{r_0}, \mathbf{z}_n) \\ &\quad - \mathcal{I}_{rn}(\mathbf{z}_{r_0}, \mathbf{z}_n) \mathcal{I}_{nn}^{-1}(\mathbf{z}_{r_0}, \mathbf{z}_n) \mathcal{I}_{rn}^T(\mathbf{z}_{r_0}, \mathbf{z}_n)) (\mathbf{z}_r - \mathbf{z}_{r_0}). \end{aligned} \quad (82)$$

Here \mathbf{z}_n are the true but unknown nuisance parameters. Under $y = 0$, the distributions of GLRT are the same in both cases. Under $y = 1$, if $\mathcal{I}_{rs} = 0$, (82) reduces to (81) and $\lambda_{\text{known}} = \lambda_{\text{unknown}}$. Thus the detection performance is the same in both cases.

D. Statistical distances and MMD

In this appendix, we provide a brief background on statistical distances. Maximum Mean Discrepancy (MMD) is a statistical distance defined as [26]:

$$d_{\text{MMD}}(X; Y) = \mathbf{E}[k(X, X')] + \mathbf{E}[k(Y, Y')] - 2\mathbf{E}[k(X, Y)] \quad (83)$$

where X and X' are independent and identically distributed (i.i.d.), and so are Y and Y' . The function $k(\cdot, \cdot)$ is a characteristic kernel over a reproducing kernel Hilbert space, e.g., the Gaussian Radial Basis Function (RBF).

Recent advances in deep generative models allow us to optimize distances as MMD in an empirical and differentiable manner [25]. For this purpose, we need to represent each distribution using samples drawn from it. Let $\{X_i\}_{i=1}^N$ and $\{Y_i\}_{i=1}^N$ be i.i.d. realizations of X and Y , respectively. Then, an empirical version of the MMD can be used where the expectations in (83) are replaced by their empirical estimates. More advanced metrics can be obtained using the tools of generative adversarial networks (GANs). In this paper, we only deal with distances between scalar random variables and simple MMD distances suffice.

REFERENCES

- [1] C. Dong, C. C. Loy, K. He, and X. Tang, “Image super-resolution using deep convolutional networks,” *IEEE transactions on pattern analysis and machine intelligence*, vol. 38, no. 2, pp. 295–307, 2015.
- [2] G. Ongie, A. Jalal, C. A. Metzler, R. G. Baraniuk, A. G. Dimakis, and R. Willett, “Deep learning techniques for inverse problems in imaging,” *IEEE Journal on Selected Areas in Information Theory*, vol. 1, no. 1, pp. 39–56, 2020.
- [3] L. Gabrielli, S. Tomassetti, S. Squartini, and C. Zinato, “Introducing deep machine learning for parameter estimation in physical modelling,” in *Proceedings of the 20th International Conference on Digital Audio Effects*, 2017.
- [4] V. Dua, “An artificial neural network approximation based decomposition approach for parameter estimation of system of ordinary differential equations,” *Computers & chemical engineering*, vol. 35, no. 3, 2011.
- [5] R. Dreifuerst and R. W. Heath Jr, “SignalNet: A low resolution sinusoid decomposition and estimation network,” *arXiv preprint arXiv:2106.05490*, 2021.
- [6] T. Diskin, Y. C. Eldar, and A. Wiesel, “Learning to estimate without bias,” *Preprint arXiv:2110.12403*, 2021.
- [7] N. Samuel, T. Diskin, and A. Wiesel, “Learning to detect,” *IEEE Transactions on Signal Processing*, vol. 67, no. 10, pp. 2554–2564, 2019.
- [8] L. Girard, V. Roy, P. Giguère, and T. Eude, “Deep neural network training using synthetic signatures for rare target detection in SWIR hyperspectral imagery,” in *2021 IEEE International Geoscience and Remote Sensing Symposium IGARSS*, pp. 4420–4423, IEEE, 2021.
- [9] A. Brighente, F. Formaggio, G. M. Di Nunzio, and S. Tomasin, “Machine learning for in-region location verification in wireless networks,” *IEEE Journal on Selected Areas in Communications*, vol. 37, no. 11, pp. 2490–2502, 2019.
- [10] D. de la Mata-Moya, M. P. Jarabo-Amores, J. M. de Nicolás, and M. Rosa-Zurera, “Approximating the Neyman–Pearson detector with 2C-SVMs. application to radar detection,” *Signal Processing*, vol. 131, pp. 364–375, 2017.
- [11] A. Ziemann, M. Kucer, and J. Theiler, “A machine learning approach to hyperspectral detection of solid targets,” in *Algorithms and Technologies for Multispectral, Hyperspectral, and Ultraspectral Imagery XXIV*, vol. 10644, p. 1064404, International Society for Optics and Photonics, 2018.
- [12] J. Theiler, S. Matteoli, and A. Ziemann, “Bayesian detection of solid subpixel targets,” in *2021 IEEE International Geoscience and Remote Sensing Symposium IGARSS*, pp. 3213–3216, IEEE, 2021.
- [13] E. Conte, A. De Maio, and C. Galdi, “CFAR detection of multidimensional signals: An invariant approach,” *IEEE Transactions on Signal Processing*, vol. 51, no. 1, pp. 142–151, 2003.
- [14] R. Kokaly, R. Clark, G. Swayze, K. Livo, T. Hoefen, N. Pearson, R. Wise, W. Benzel, H. Lowers, R. Driscoll, *et al.*, “USGS spectral library version 7 data: US geological survey data release,” *United States Geological Survey (USGS): Reston, VA, USA*, 2017.
- [15] A. Coluccia, A. Fascista, and G. Ricci, “Design of customized adaptive radar detectors in the CFAR feature plane,” *arXiv preprint arXiv:2203.12565*, 2022.
- [16] S. Kay, *Fundamentals of Statistical Signal Processing: Detection theory*. Fundamentals of Statistical Si, Prentice-Hall PTR, 1998.
- [17] A. Herschtal and B. Raskutti, “Optimising area under the ROC curve using gradient descent,” in *Proceedings of the twenty-first international conference on Machine learning*, p. 49, 2004.
- [18] U. Brefeld, T. Scheffer, *et al.*, “AUC maximizing support vector learning,” in *Proceedings of the ICML 2005 workshop on ROC Analysis in Machine Learning*, 2005.
- [19] H. Narasimhan and S. Agarwal, “A structural SVM based approach for optimizing partial AUC,” in *International Conference on Machine Learning*, pp. 516–524, PMLR, 2013.
- [20] P. Braca, L. M. Millefiori, A. Aubry, S. Marano, A. De Maio, and P. Willett, “Statistical hypothesis testing based on machine learning: Large deviations analysis,” *arXiv preprint arXiv:2207.10939*, 2022.
- [21] C.-H. Lin, Y.-C. Lin, Y. Bai, W.-H. Chung, T.-S. Lee, and

H. Huttunen, “DL-CFAR: A novel cfar target detection method based on deep learning,” in *2019 IEEE 90th Vehicular Technology Conference (VTC2019-Fall)*, pp. 1–6, IEEE, 2019.

[22] J. Akhtar and K. E. Olsen, “A neural network target detector with partial CA-CFAR supervised training,” in *2018 International Conference on Radar (RADAR)*, pp. 1–6, IEEE, 2018.

[23] J. Akhtar, “Training of neural network target detectors mentored by SO-CFAR,” in *2020 28th European Signal Processing Conference (EUSIPCO)*, pp. 1522–1526, IEEE, 2021.

[24] I. Goodfellow, J. Pouget-Abadie, M. Mirza, B. Xu, D. Warde-Farley, S. Ozair, A. Courville, and Y. Bengio, “Generative adversarial nets,” *Advances in neural information processing systems*, vol. 27, 2014.

[25] Y. Li, K. Swersky, and R. Zemel, “Generative moment matching networks,” in *International conference on machine learning*, pp. 1718–1727, PMLR, 2015.

[26] A. Gretton, K. M. Borgwardt, M. J. Rasch, B. Schölkopf, and A. Smola, “A kernel two-sample test,” *The Journal of Machine Learning Research*, vol. 13, no. 1, pp. 723–773, 2012.

[27] E. J. Kelly, “An adaptive detection algorithm,” *IEEE transactions on aerospace and electronic systems*, no. 2, pp. 115–127, 1986.

[28] F. C. Robey, D. R. Fuhrmann, E. J. Kelly, and R. Nitzberg, “A CFAR adaptive matched filter detector,” *IEEE Transactions on aerospace and electronic systems*, vol. 28, no. 1, pp. 208–216, 1992.

[29] E. Conte, M. Lops, and G. Ricci, “Adaptive matched filter detection in spherically invariant noise,” *IEEE Signal Processing Letters*, vol. 3, no. 8, pp. 248–250, 1996.

[30] D. G. Manolakis, C. Siracusa, D. Marden, and G. A. Shaw, “Hyperspectral adaptive matched-filter detectors: Practical performance comparison,” in *Algorithms for Multispectral, Hyperspectral, and Ultraspectral Imagery VII*, vol. 4381, pp. 18–33, SPIE, 2001.

[31] O. Ledoit and M. Wolf, “A well-conditioned estimator for large-dimensional covariance matrices,” *Journal of multivariate analysis*, vol. 88, no. 2, pp. 365–411, 2004.

[32] Y. I. Abramovich, N. K. Spencer, and A. Y. Gorokhov, “Modified GLRT and AMF framework for adaptive detectors,” *IEEE Transactions on Aerospace and Electronic Systems*, vol. 43, no. 3, pp. 1017–1051, 2007.

[33] M. Arjovsky, L. Bottou, I. Gulrajani, and D. Lopez-Paz, “Invariant risk minimization,” *arXiv preprint arXiv:1907.02893*, 2019.

[34] Y. Wald, A. Feder, D. Greenfeld, and U. Shalit, “On calibration and out-of-domain generalization,” *arXiv preprint arXiv:2102.10395*, 2021.

[35] Y. Romano, S. Bates, and E. Candes, “Achieving equalized odds by resampling sensitive attributes,” *Advances in Neural Information Processing Systems*, vol. 33, pp. 361–371, 2020.

[36] R. Wong, *Asymptotic approximations of integrals*. SIAM, 2001.

[37] L. Tierney and J. B. Kadane, “Accurate approximations for posterior moments and marginal densities,” *Journal of the american statistical association*, vol. 81, no. 393, pp. 82–86, 1986.

[38] A. Azevedo-Filho and R. D. Shachter, “Laplace’s method approximations for probabilistic inference in belief networks with continuous variables,” in *Uncertainty proceedings 1994*, pp. 28–36, Elsevier, 1994.

[39] O. E. Barndorff-Nielsen and D. R. Cox, *Asymptotic techniques for use in statistics*, vol. 11. Springer, 1989.

[40] P. L. Bartlett, M. I. Jordan, and J. D. McAuliffe, “Convexity, classification, and risk bounds,” *Journal of the American Statistical Association*, vol. 101, no. 473, pp. 138–156, 2006.

[41] S. Shalev-Shwartz and S. Ben-David, *Understanding machine learning: From theory to algorithms*. Cambridge university press, 2014.

[42] A. P. Dempster, N. M. Laird, and D. B. Rubin, “Maximum likelihood from incomplete data via the em algorithm,” *Journal of the Royal Statistical Society: Series B (Methodological)*, vol. 39, no. 1, pp. 1–22, 1977.

[43] S. M. Kay and S. M. Kay, *Fundamentals of statistical signal processing: estimation theory*, vol. 1. Prentice-hall Englewood Cliffs, NJ, 1993.

[44] B. Bilodeau, A. Stringer, and Y. Tang, “Stochastic convergence rates and applications of adaptive quadrature in bayesian inference,” *Journal of the American Statistical Association*, pp. 1–11, 2022.

[45] B. Bilodeau, Y. Tang, and A. Stringer, “On the tightness of the laplace approximation for statistical inference,” *arXiv preprint arXiv:2210.09442*, 2022.